Elasto-plastic model for sand including time effect

B Cazacliu

LUNAM Université, IFSTTAR, MAST, GPEM, F-44340 Bouguenais, France

E Ibraim

Department of Civil Engineering, University of Bristol, Bristol, UK

Abstract. Time effects on granular soils have been observed in laboratory and in situ tests but cannot be reproduced by classical elasto-plastic models. To address these concerns, existing specific modelling approaches were based on the theory of viscoplasticity formulated by Perzyna or on a viscous evanescent relationship. The present work explores an alternative following an elasto-plastic modelling framework formulated in a multi-axial structure space. The proposed elasto-plastic model is associated with a thixotropic-type framework through the use of a structure parameter, the evolution of which illustrates the competition between two effects: the time-dependent tendency of the granular system to reach its stable configuration – restructuration – and its destructuration under external perturbations. The structure parameter is linked to the existence of a stress dependent target structure towards which the current granular material structure evolves. The time scale is explicitly introduced by postulating a rate for this structure evolution. The modelling of the material behaviour has shown good similarities with the response of granular soils observed in monotonic loading, as well as during creep and variable strain rate loading experiments.

Constitutive relations; Sands; Time dependence; Fabric/structure of soils; Elasto-plasticity

INTRODUCTION

Time effects on granular soils - time dependent strains under constant stress (creep), time dependent reduction of stresses under constant strain (relaxation) and rate dependency - have been observed in laboratory tests by Lacerda and Houston (1973), Murayama et al. (1984), Delage et al. (1990), Lade (1994), Tatsuoka et al. (1997), Di Benedetto and Tatsuoka (1997), (2002), Cazacliu and Di Benedetto (1997), Matsushita et al. (1999), Di Benedetto et al. (1999), (2005), Howie et al.

(2002), Kuwano and Jardine (2002), Bowman and Soga (2003), Van Bang et al. (2007) but also on some field applications reported by Mitchell & Solymar (1984), Mesri et al. (1990), Schmertmann (1991), Jardine et al. (2006). The soil response is affected by the extent of time over which the effective stress (or strain) has been sustained. Concerning the rate dependency, tests on sand conducted at different constant strain rates (within laboratory testing capabilities) showed minor differences, mainly within the experimental repeatability range (Matsushita et al., 1999). In contrast, if the strain rate is suddenly changed stepwise either increased or decreased, the stress-strain relationship temporarily either overshoots or undershoots before progressively re-joining the curve response for the constant strain rate.

The time effects on sands cannot be reproduced by classical elasto-plastic models and different modelling approaches have emerged to include the observed time-dependent behaviour. One approach, offered by Di Prisco and Imposimato (1996), Imposimato et al. (2000), refers to and is based on the theory of viscoplasticity formulated by Perzyna (1966). Alternatively, Di Benedetto and Tatsuoka (1997), Tatsuoka et al. (1999), Di Benedetto et al. (2001), (2002) proposed a viscous evanescent relationship within a general three-component model framework, recently implemented in finite element method code (Peng et al, 2010).

Unless particle crushing occurs, no clear physical justification is given to explain the fundamentals of the time effect mechanisms. However, macro-response observations on sand under stresses (creep) or strains (relaxation) left unchanged over time show, under subsequent reloading, an increase in stiffness and strength, and apparent signs of erasure of the stress and strain histories (Ibraim et al. 2009). These suggest that a continuous relative rearrangement of the individual particles occurs towards a more stable structure configuration (Delage et al. 1990, Schmertmann, 1991, Di Prisco and Imposimato, 1996, Bowman and Soga, 2003, Miksic and Alava, 2013). The particle rearrangement mechanism, although of unknown origin, should be bounded by the accessible geometrical constraints of the system and thus is relatively limited – as also observed in experiments.

Based on this context, the present work explores ways to incorporate the time-dependency of sand behaviour into a classical elasto-plastic modelling framework for sands. A rearrangement mechanism of the granular material structure towards a target structure is assumed. By postulating a rate for this structural evolution, the time scale is explicitly introduced; this subsequently allows the study of its influence

on the granular media loading processes. The model simulations focus mainly on the response of granular soils in monotonic loading, including creep stages and rate dependency effects.

CONSTITUTIVE MODEL

Classic elasto-plastic model formulations have adopted the conventional stress space framework, but developments have also been conducted in the strain space (Einav and Carter, 2007). In this work, the model is formulated in a *structure space* defined as an isomorphic transformation (Mac Lane, 1971) of the stress space.

The elasto-plastic model is associated here with a thixotropic-type framework (Coussot, 2007), by considering a *structure parameter* (of tensorial form) the evolution of which illustrates the competition between two effects: the continuous tendency of the system to reach its stable configuration – restructuration – and its destructuration under shear. The decrease of the structure parameter corresponds to restructuration, while destructuration implies its increase under perturbations. The usual thixotropic macroscopic models take the form of a shear stress vs. shear strain rate relation in which the parameters depend on a variable describing the actual state of the structure. In this context, the variable (structure parameter) evolves with the flow history, an effect which is generally described with the help of a kinetic equation expressing its current rate of variation as a function of its current value and the current shear strain rate (Coussot, 2007). In the present approach, the tensor structure evolution rate depends on its current value and on the current stress rate.

Structure space

The *structure space* is defined as a 3-dimensional space with the axes representing the three principal directions of a material structure tensor. In this development we adopt the formulation of the second-order structure tensor, N_{ij}, used by Radjai et al. (2012), which associates the coordination number and the structure tensor as defined by Satake (1982):

$$N_{ij} = n\int_{\Omega} \xi_i \xi_j E(\xi) d\xi \qquad (1)$$

where ξ_i is the inter-particle contact normal in the *i*-direction, $E(\xi)$ is the contact normal distribution function (spatial probability density function of ξ), Ω is the space of contact orientations. $n = tr\left(N_{ij}\right)$ designates the coordination number, half of the average number of contacts per particle. N_{ij} eigenvalues could be considered as representative indicators for structure intensity over the principal directions (Maeda and Ibraim, 2008).

Destructuring / restructuring framework

We introduce a target stress state dependent structure tensor, $N_{ij\infty}$. It is further assumed that the current material structure tensor, N_{ij}, tends in time towards the target structure, in line also with the work of Richard et al. (2005). This is expressed here as:

$$\dot{N}_{ij} = \lambda\left(N_{ij\infty} - N_{ij}\right) = \lambda \cdot \Gamma_{ij} \qquad (2)$$

where λ is a material constant and $\Gamma_{ij}(N_{ij})$ is the structure parameter tensor defined by the distance between the target and the current structure.

If the stress state changes, the target structure, $N_{ij\infty}$, instantaneously changes and the structure parameter, Γ_{ij}, generally increases; this describes the destructuration mechanism. At sufficiently low stress rates, the structure parameter tensor decreases, and relation (2) characterises the restructuring mechanism. This decrease, of $e^{-\lambda t}$ type, explicitly introduces the physical time dimension into the problem. λ is the inverse of the half-life time of the evolution of the structure tensor, N_{ij}, towards the target structure, $N_{ij\infty}$.

One relatively simple relation of the target structure tensor and its evolution with the change in the current stress is given based on the following two assumptions:

(i) proportionality of the target structure tensor with the power *m* of the current stress state tensor:

$$N_{ij\infty} = \frac{n_\infty}{tr\left(\sigma_{ij}{}^m\right)}\sigma_{ij}{}^m \qquad (3)$$

where $n_\infty = tr(N_{ij\infty})$ is the target coordination number, tr($\bullet$) indicates the trace of the tensor $\bullet$ and *m* is a material constant which controls the evolution of the distortional part of the target structure, $N_{ij\infty}$, with the distortional part of the stress σ_{ij}. Taking into account relation (2), the relation (3) implies that the principal directions of the current structure tensor follow the directions of the stress tensor. *m* < 1 restrains the evolution of the target structure tensor.

(ii) proportionality between:

(a) $n_\infty - n_{cr}$, the difference between the target coordination number and the coordination number at the critical state, n_{cr}, and

(b) $\eta_\infty \pm \eta_{\max}$, the distance between a hardening variable associated to the target structure state, η_∞, and a failure limit in the direction of loading, $\pm\eta_{\max}$.

Incrementally, the proportionality condition (ii) yields:

$$\dot{n}_\infty = \frac{n_\infty - n_{cr}}{\eta_\infty - sig(\dot{\eta}_\infty)\eta_{\max}} \dot{\eta}_\infty \qquad (4)$$

The relation (4) suggests that the target coordination number, n_∞, converges monotonically towards the coordination number at the critical state, n_{cr}, once η_∞ changes. If η_∞ does not change, for instance during creep tests, n_∞ remains unchanged. In this approach, the failure limit $\eta_{\max}$ is assumed state independent, and confounded with the value of the hardening variable at the critical state.

Elasto-plastic framework

The strain rate follows the classical decomposition into elastic, $\dot{\varepsilon}_{ij}^{\ e}$, and plastic, $\dot{\varepsilon}_{ij}^{\ p}$, incremental strain rate tensors:

$$\dot{\varepsilon}_{ij} = \dot{\varepsilon}_{ij}^{\ e} + \dot{\varepsilon}_{ij}^{\ p} \qquad (5)$$

The elastic strain response is defined as follows:

$$\dot{\varepsilon}_{ij}^{\ e} = C_{ijkl}\dot{\sigma}_{kl} \qquad (6)$$

where C_{ijkl} is the elastic compliance fourth-order tensor and $\dot{\sigma}_{kl}$ is the stress rate tensor.

The yield surface and limit surface are defined in the structure space, following a Drucker-Prager type criterion:

$$f_y\left(N_{ij},\eta\right)=\tfrac{1}{\sqrt{3}}\left(n_q-n_p\,\eta\right) \tag{7}$$

where η is the hardening variable which indicates the current size of the yield locus and $n_p=\tfrac{1}{3}I_1\left(N_{ij}\right)$ and $n_q=\sqrt{\tfrac{2}{3}J_2\left(N_{ij}\right)}$. $I_1(\bullet)$ represents the first invariant of the tensor $\bullet$, while $J_2(\bullet)$ is the second invariant of its deviatoric part. The hardening variable progressively increases with the monotonic shear loading until the loading direction is changed or up to a fixed limiting value, $\eta_{\max}$. The latter takes place when the yield surface reaches the failure surface limit:

$$F\left(N_{ij},\eta_{\max}\right)=\tfrac{1}{\sqrt{3}}\left(n_q-n_p\,\eta_{\max}\right) \tag{8}$$

The flow rule that describes the mechanism of plastic deformation is:

$$\dot{\varepsilon}_{ij}^{\,p}=\mu\frac{\partial g\left(N_{ij}\right)}{\partial N_{ij}} \tag{9}$$

where *g* is the plastic potential function and μ is a scalar multiplier. The plastic potential function, *g*, is defined in the structure space:

$$g\left(N_{ij}\right)=\Gamma_{ij}\Gamma_{ij} \tag{10}$$

where $\Gamma_{ij}\left(N_{ij}\right)$ is the *structure parameter* tensor. The plastic potential function is the square of the distance between the current structure tensor and the target structure tensor. The choice of (10) provides a way to insure proportionality between the plastic strain increment and the current structure increment.

Finally, the hardening rule assumes that the current size of the yield locus, η, depends only on the plastic distortional strain, $\varepsilon_q^{\,p}$, through a very simple monotonic hyperbolic relationship that captures the soil stiffness degradation under monotonic

loading (Muir Wood, 2004):

$$\frac{\eta}{\eta_{\max}} = \frac{\varepsilon_q^p}{a + \varepsilon_q^p} \tag{11}$$

which becomes in an incremental form:

$$\dot{\varepsilon}_q^p = \frac{a\eta_{\max}}{\left(\eta_{\max} - \eta\right)^2}\dot{\eta} \tag{12}$$

a in the relation (11) is a material constant which scales the plastic distortional strain. The plastic distortional strain is $\varepsilon_q^p = \sqrt{\frac{2}{3} J_2\left(\varepsilon_{ij}{}^p\right)}$.

Figure 1 gives a graphic description of the yield and plastic potential functions in the meridian structure plane, including the structure, target structure and their evolutions. In an incremental time:

- the structure evolves incrementally, δN_{ij}, in the direction of the current target structure, $N_{ij\infty}$; the hardening parameter, η, changes;
- the associated increment of stress produces an incremental evolution of the target structure, $\delta N_{ij\infty}$; n_∞ evolves towards n_{cr};
- the structure parameter, Γ_{ij}, is the distance between N_{ij} and $N_{ij\infty}$.

Strain rate

By introducing (3) in relation (10) and using (2) one can deduce that:

$$\dot{\varepsilon}_{ij}{}^p = 2\lambda\mu\dot{N}_{ij} \tag{13}$$

Based on this relation, one can obtain the plastic distortional strain rate (12) and determine μ to completely define the plastic compliance relationship linking plastic strain rate with the structure evolution:

$$\dot{\varepsilon}_{ij}{}^p = \frac{a\eta_{\max}}{\left(\eta_{\max} - \eta\right)^2}\frac{\dot{\eta}}{\dot{n}_q}\dot{N}_{ij} \tag{14}$$

where the rate of the hardening parameter, $\dot{\eta}$, is determined by the consistency rule,

after developing (8):

$$\dot{\eta} = \frac{\dot{n}_q - \eta\, \dot{n}_p}{n_p} \tag{15}$$

Introducing (14) and (7) in relation (6) we obtain the final expression of the strain rate response:

$$\dot{\varepsilon}_{ij} = C_{ijkl}\dot{\sigma}_{kl} + \frac{a\eta_{\max}}{(\eta_{\max} - \eta)^2}\frac{\dot{\eta}}{\dot{n}_q}\dot{N}_{ij} \tag{16}$$

Figure 2 presents the flow chart of the model in stress-controlled mode.

SIMULATIONS

A few examples based on drained triaxial axisymmetric test conditions to illustrate the features embedded in the proposed model are given. In the present development, the model uses 7 parameters: 2 for the elastic ($E_{\max}$ and ν) and 2 for the plastic ($\eta_{\max}$ and a) behaviours, 2 for the target structure (m and n_{cr}) and one for the restructuration mechanism (λ). In these simulations, loose and dense sand conditions are defined by initial coordination numbers, n_o, ±2.5% or ±5% lower and higher, respectively, than the critical coordination number, n_{cr}. For simplicity, the parameters a and ν are kept unchanged for both loose and dense sands, while $\eta_{\max}$ takes a range of values that would correspond to a series of angles of friction between 34° and 43°. The relationship between E_{max} and the initial coordination number simply follows an arbitrary increasing function. The values of m and λ are 0.33 and $0.14 \times 10^{-3}\ s^{-1}$, respectively. No inherent anisotropy of samples is considered and time-effects are assumed to be fully consumed at the beginning of the tests ($\Gamma_{ij\,0} = 0$).

Typical simulation results in monotonic triaxial loading in compression and extension (loading rate of 2.7 kPa/s) at a lateral constant confining pressure of 100 kPa are shown in Figure 3: axial stress and volumetric strain versus axial strain. The tendencies of stress-strain and volumetric strain thus obtained correlate qualitatively well with known response of granular material. The volumetric response in

compression is density dependent and shows initial densification followed by either dilatancy for dense sand or by further densification for loose packing structure. For the extension loading case, the volumetric response is initially dilative for all densities and it indicates a continuous response of the granular material from compression to extension at the same initial isotropic stress state. Further loading produces the same volumetric pattern response as in compression, density dependent.

Figure 4 shows stress-controlled triaxial compression tests (loading rate 1.3 kPa/s) four on identical loose (n_o = 0.95 n_{cr}) and four tests on dense (n_o = 1.05 n_{cr}) sand samples. In each case, three tests were stopped at different axial stress and creep tests were performed over identical time periods. As similarly observed in experiments (Murayama et al. 1984, Delage et al. 1990, Mejia and Vaid, 1988, Di Benedetto and Tatsuoka, 1997, Tatsuoka et al. 2002) creep deformation is occurring and its amount is a function of the stress level at which the creep test is performed: the higher the stress level, the higher the creep strain. The curves of volumetric strain recorded during creep prolong the curve obtained during the monotonic loading, while the stress-strain curves after the creep stages converge towards the monotonic one. The evolution of the axial strain with the logarithm of time reproduces well the experimentally observed trends (Figure 5). For creep tests performed at the same hardening to maximum hardening ratio, time effects are much more pronounced as sample density decreases.

Four stress-controlled triaxial compression tests on loose samples with creep tests performed at similar deviator stress, but under different creep times, are presented on Figure 6. The material stiffness after reloading increases with the creep time, in agreement with experimental observations. The influence of the rate dependency is studied in the Figure 7. If the strain rate is suddenly changed stepwise, either becoming faster or slower, the stress-strain relationship temporarily either overshoots or undershoots before progressively re-joining the relationship for the constant rate of strain (Figure 7a). Triaxial test simulations at different constant strain rates (Figure 7b) show minimal differences in the stress-strain and volumetric responses, also in line with experimental results.

CONCLUSIONS

The present work has explored ways to model the experimentally observed time-dependency behaviour of granular soils. The model, based on a classical elasto-plastic framework, is formulated in a multi-axial *structure* space. The elasto-plastic model was associated with a thixotropic-type framework through the use of a structure parameter. The evolution of the structure parameter describes the competition between two effects: the time-dependent tendency of the granular system to reach its stable configuration – restructuration – and its destructuration under external perturbations. The structure parameter is linked to the existence of a granular material target structure towards which the current structure evolves asymptotically. The target structure is supposed to be related to the current stress state. The time scale is explicitly introduced by postulating a rate for this structure evolution. Despite its reduced number of parameters, the simulations qualitatively captured the peculiarities of the observed response of granular soils in triaxial experiments. Multi-axial loading conditions including rotation of principal axes will be explored in subsequent work.

Further model developments for phenomena that cannot be captured by the present form, include: (i) the dependency of the elastic constants and the scaling plastic distortional strain parameter, a, on the current structure, stress and density; (ii) post-peak softening and tertiary creep responses by introducing the dependency of the maximum hardening variable on the current void ratio; (iii) isotropic plastic effects by dependency of critical coordination number on the current stress state. The dependency of the characteristic time, $1/\lambda$, on the internal kinetic energy of the granular packing could also be explored.

ACKNOWLEDGEMENT

The authors gratefully acknowledge the support provided by the UK Royal Academy of Engineering under the Newton Research Collaboration Programme and La Région Des Pays de la Loire, France.

REFERENCES

Bowman, E.T. & Soga, K. (2003). Creep, ageing and microstructural change in dense granular materials. *Soils and Foundations*, **43**(4), 107-117.

Cazacliu, B. & Di Benedetto, H. (1998) Nouvel essai sur cylindre creux de sable. *Revue Française de Génie Civil*, Vol. **2**, No. 7, 825-855.

Coussot, P. (2007). Rheophysics of Pastes: A Review of Microscopic Modelling Approaches. *Soft Matter* **3**, No. 5 528-540

Delage, P., Noc X., Saidy, G. & De Laure, E. (1990) Aspects volumiques du fluage des sables. *Proc. 25ème Colloque du Groupe Français de Rhéologie, Grenoble : Institut Mécanique*, 147-158.

Di Benedetto, H. & Tatsuoka, F. (1997) Small strain behavior of geomaterials: modelling of strain rate effects. *Soils and Foundations*, **37**(2), 127-138.

Di Benedetto, H., Ibraim, E. & Cazacliu, B. (1999). Time dependent behaviour of sand. *Proc. of 2nd Int. Symp. on Pre-failure Def. Characteristics of Geomaterials*, *Torino*, Jamiolkowski M et al. (eds), vol. 1, 459-466.

Di Benedetto H, Sauzéat C, Goeffroy H. (2001) Modelling viscous effects and behaviour in the small strain domain. *Proc. of 2nd Int. Symp. on Pre-failure Def. Characteristics of Geomaterials*, *Torino*, Jamiolkowski M et al. (eds), vol. 2, 1357–1367.

Di Benedetto, H. & Tatsuoka, F. (2002) Time-dependent deformation charcateristics of sand and their constitutive modelling. *Soils and Foundations*, **42**(2), 1-22.

Di Benedetto H, Tatsuoka F, Lo Presti D, Sauzéat C, Geoffroy H. (2005) Time effects on the behaviour of geomaterials. Keynote Lecture *IS Lyon03, Deformation Characteristics of Geomaterials: Recent Investigations and Prospects*, Di Benedetto H. et al. (eds). Balkema: Rotterdam.

Di Prisco, C. & Imposimato, S. (1996) Time dependent mechanical behaviour of loose sands. *Mechanics of Cohesive-Frictional Materials*, **1**, 45-73

Di Prisco, C., Imposimato, S. & Vardoulakis, I. (2000) Mechanical modelling of drained creep triaxial tests on loose sand. *Géotechnique* **59**, No. 1, 73-82.

Einav, I. & Carter, J. (2007). On convexity, normality, pre-consolidation pressure and singularities in modelling of granular materials. *Granular Matter*, **9**(1-2), 87-96.

Howie, J.A., Schozen, T. & Vaid, Y.P. (2002) Effect of ageing on stiffness of very loose sand. *Canadian Geotech. J.*, **39**, 149-156.

Ibraim E., Di Benedetto H. & Doanh. T. (2009) Time-dependent behaviour and static liquefaction phenomenon of sand. *Geotechnical and Geological Engineering Journal*, **27**, 181 – 191.

Jardine, R.J., Standing, J.R. & Chow, F.C. (2006) Some observations of the effects of time on the capacity of piles driven in sand, *Géotechnique* **56**, No. 4, 227-244.

Kuwano, R. & Jardine, J. (2002). On measuring creep behaviour in granular materials through triaxial testing. *Canadian Geotech. J.*, **39**, 1061-1074.

Lacerda, W.A. & Houston, W.N. (1973) Stress relaxation in soils, in *Proceedings of the VIIIth Int. Conf. on Soil Mechanics and Foundation Engng.*, Moscow, 1, 221-227.

Lade, P. V. (1994) Creep Effects on Static and Cyclic Instability of Granular Soils. *J. of Geotech. Eng.*, **120**(2), 404-419.

Mac Lane S. (1971), Categories for the Working Mathematician, Springer Verlag, Berlin

Maeda, K. & Ibraim, E. (2008) DEM analysis of 2D fibre-reinforced granular soils. *Proc. of 4th Int. Symp. on Pre-failure Def. Characteristics of Geomaterials*, *Atlanta*. Burns, S. E., Mayne, P. W. & Santamarina, J. C. (eds.). IOS Press, Vol. Vol. 2, 623-628.

Matsushita M., Tatsuoka K., Koseki J., Cazacliu B., Di Benedetto H., Yasin S.J.M. (1999) Time effect on the pre-peak deformation properties of sands. *Proc. of 2nd Int. Symp. on Pre-failure Def. Characteristics of Geomaterials*, *Torino*, Jamialkowski et al. eds, Balkema, Vol.1, 681-689.

Mejia, C.A. & Vaid, Y.P. (1988) Time dependent behaviour of sand. Proceedings of the Int. Conf. on Rheology and Soil Mechanics, Coventry, UK, September, Ed. M.J. Keedwell, 312-326.

Mesri, G., Feng, T.W. & Benak, J.M. (1990). Postdensification Penetration Resistance of Clean Sands *Journal of the Geotechnical Engineering Division, ASCE,*, 116(7), pp. 1095-1115

Mitchell, J.K. & Solymar, Z.V. (1984). Time-Dependent Strength Gain in Freshly Deposited or Densified Sand, *Journal of Geotechnical Engineering*, **110**, No. 11, 1559-1576.

Miksic, A. & Alava, M.J. (2013). Evolution of grain contacts in a granular sample under creep and stress relaxation. Physical Review E, **88**(3), 1-7.

Mohkam M (1983) Contribution a l'étude expérimentale et théorique du comportement des sables sous chargements cycliques. PhD thesis, USM Grenoble, France.

Muir Wood, D. (2004). *Geotechnical Modelling*. 1st Edition, Spon Press. 480p.

Murayama, S., Michihiro, K. & Sakagami, T. (1984) Creep characteristics of sands, *Soils and Foundations*, **24**(2), 1-15.

Peng F-L, Li, F-L, Tan, Y & Kongkitkul, W. (2010). FEM simulations of viscous properties for granular materials considering the loading rate effect. *Granular Matter*, **12**, 555-568.

Perzyna, P. (1966). Fundamental problems in viscoplasticity, *Advances in Applied Mechanics*, Vol. 9, Academic Press, 243-377.

Richard, P., Nicodemi, M., Delannay, R., Ribiere, P., & Bideau, D. (2005). Slow Relaxation and Compaction of Granular Systems. *Nature Materials* **4**, No. 2, 121–128.

Radjai, F., Delenne, J.-Y., Azéma, E. & Roux, S. (2012). Fabric Evolution and Accessible Geometrical States in Granular Materials. *Granular Matter* **14**, No. 2, 259–64.

Satake, M. (1982). Fabric tensor in granular materials. *Proc. IUTAM-Conference on Deformation and Failure of Granular Materials*, 63-68.

Schmertmann, J.H. (1991) The mechanical aging of soils. *J. of Geotech. Engng.*, **117(**9), pp. 1288-1330

Tatsuoka, F., Jardine, R.J., Lo Presti, D., Di Benedetto, H. & Kodaka, T. (1997) Characteristing of the Pre-Failure Deformation Properties of Geomaterials. *Proc. XIVth Int. Conf. on Soil Mechanics and Foundation Engineering*, Hamburg, 35p.

Tatsuoka F, Ishihara M, Di Benedetto H, Kuwano R. (2002) Time dependent shear deformation characteristics of geomaterials and their simulation. *Soils and Foundations*, **42**(2), 103–129.

Tatsuoka F., Uchimura T., Hayano K., Di Benedetto H., Koseki J. & Siddiquee M.S.A. (1999) Time dependent deformation characteristics of stiff geomaterials in engineering practice. IS Torino: Theme Lecture in *Proceedings of Second IS on Pre Failure Deformation Characteristics of Geomaterials*, Vol. 2, 1161–1262.

Van Bang, D.P., Di Benedetto, H., Duttine, A. & Ezaoui, A. (2007) Viscous behaviour of dry sand. *International Journal for Numerical and Analytical Methods in Geomechanics*, **31**, Issue 15, 1631–1658.

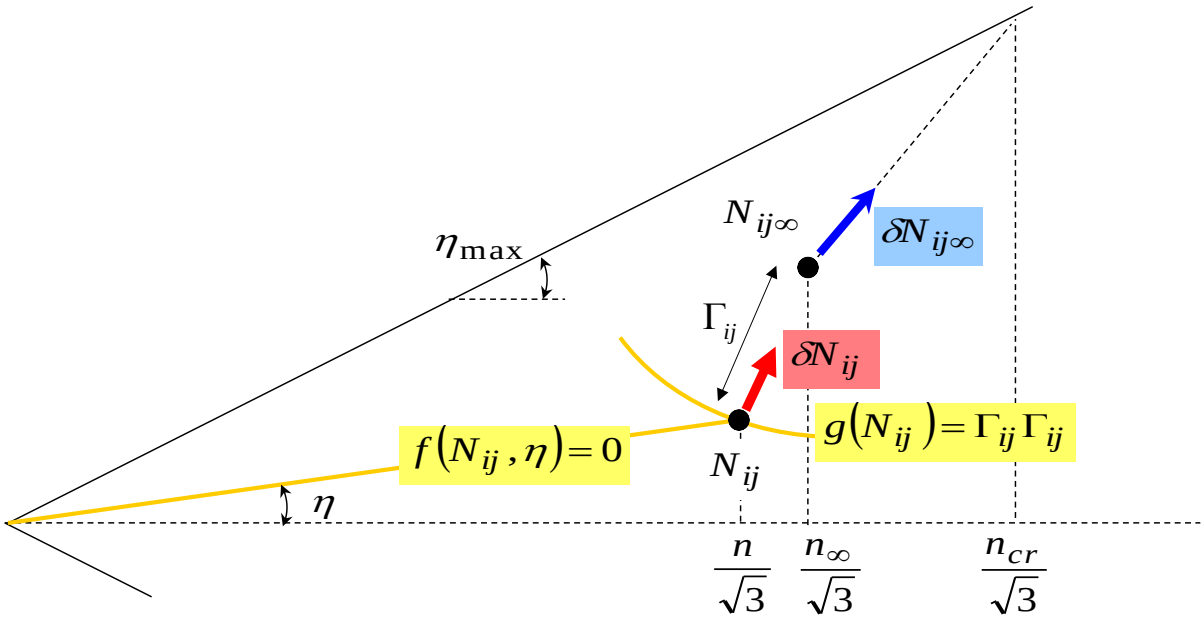

Meridian structure plane

Figure 1. Schematic presentation of the yield and potential functions in the meridian structure plane, including the structure, target structure and their incremental evolution, $\delta N_{ij\infty}$ and δN_{ij}.

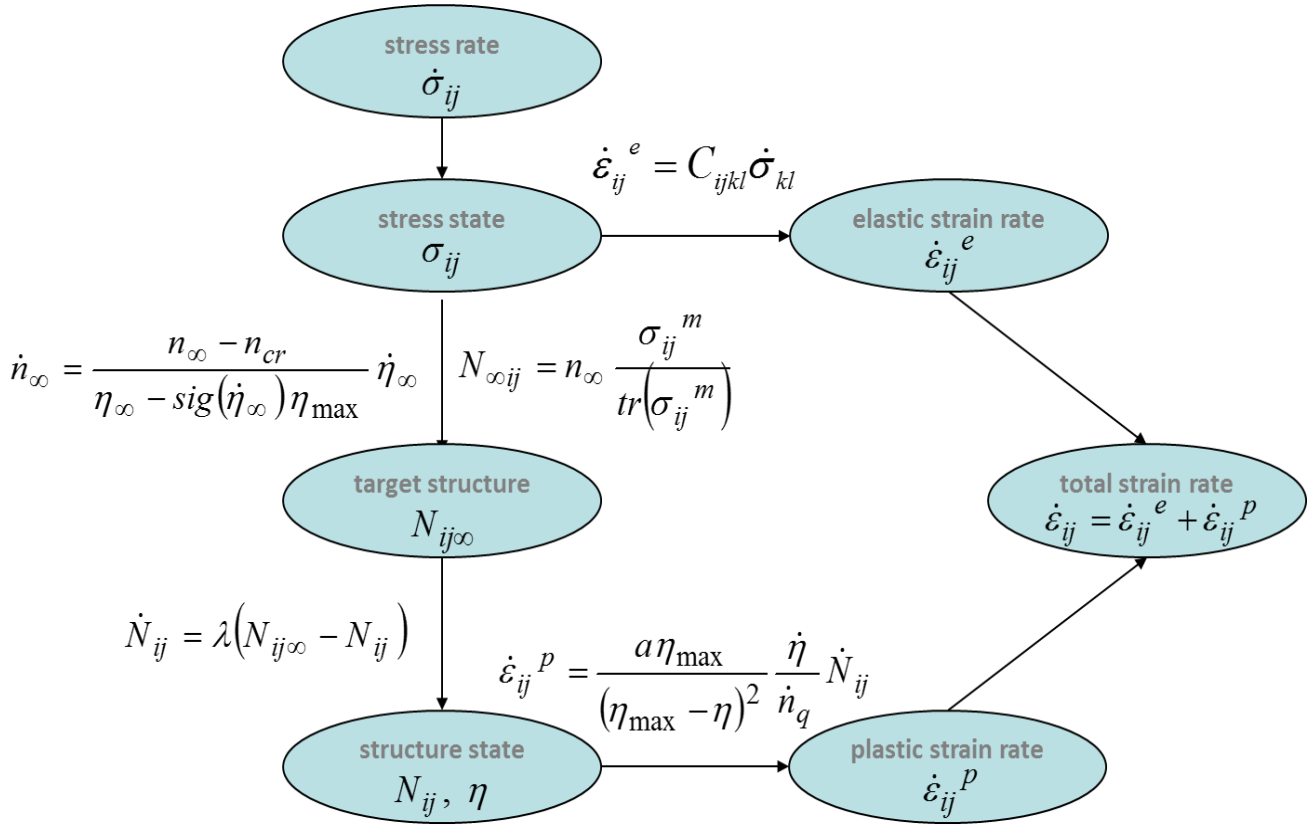

Figure 2. Flow chart of the model.

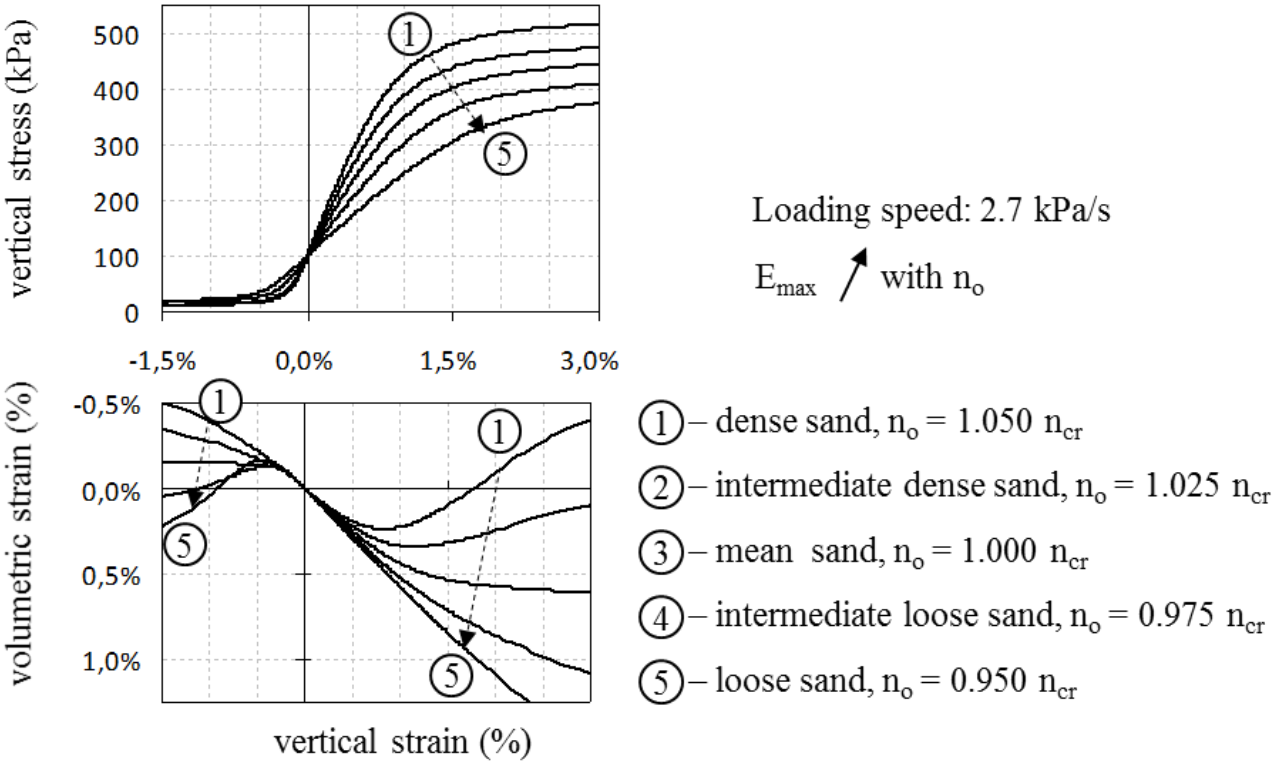

Figure 3. Typical simulation results of monotonic triaxial loading in compression and extension (loading rate of 2.7 kPa/s) at constant lateral confining pressure of 100 kPa.

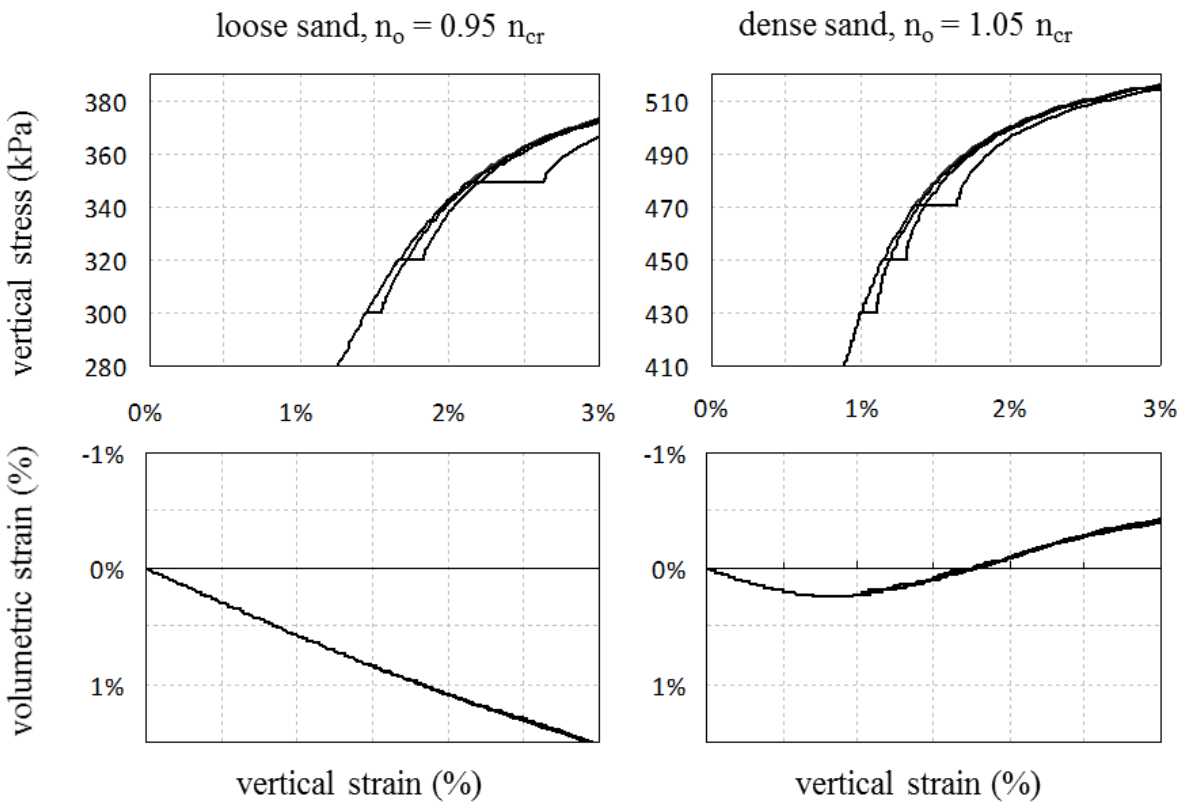

Figure 4. Stress-controlled triaxial compression tests (loading rate 1.3 kPa/s) on initially identical loose (n_o = 0.95 n_{cr}) and dense (n_o = 1.05 n_{cr}) sand at constant lateral confining pressure of 100 kPa; creep test of identical time performed at different vertical stress levels.

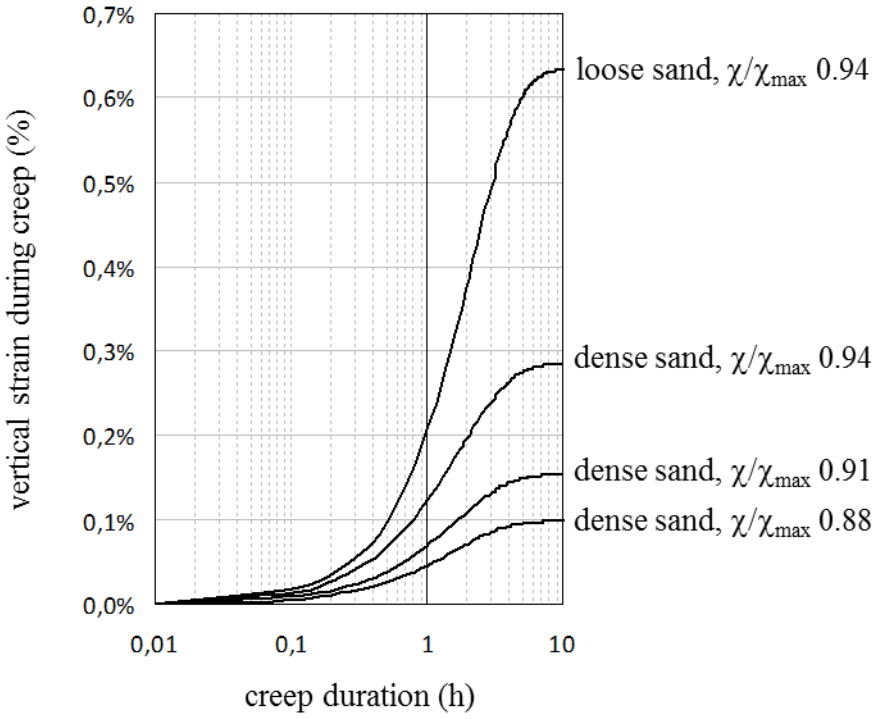

Figure 5. Evolution of the axial strain with the logarithm of time during creep for the tests presented in Figure 4; $\eta / \eta_{\max}$ indicates the hardening to maximum hardening ratio at each corresponding creep level.

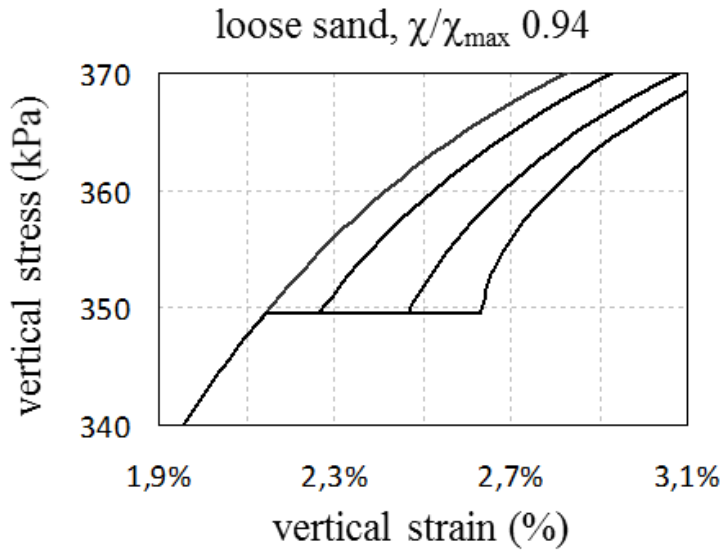

Figure 6. Stress-controlled triaxial compression tests at constant lateral confining pressure of 100 kPa with creep periods performed at similar deviator stress, but with different creep time

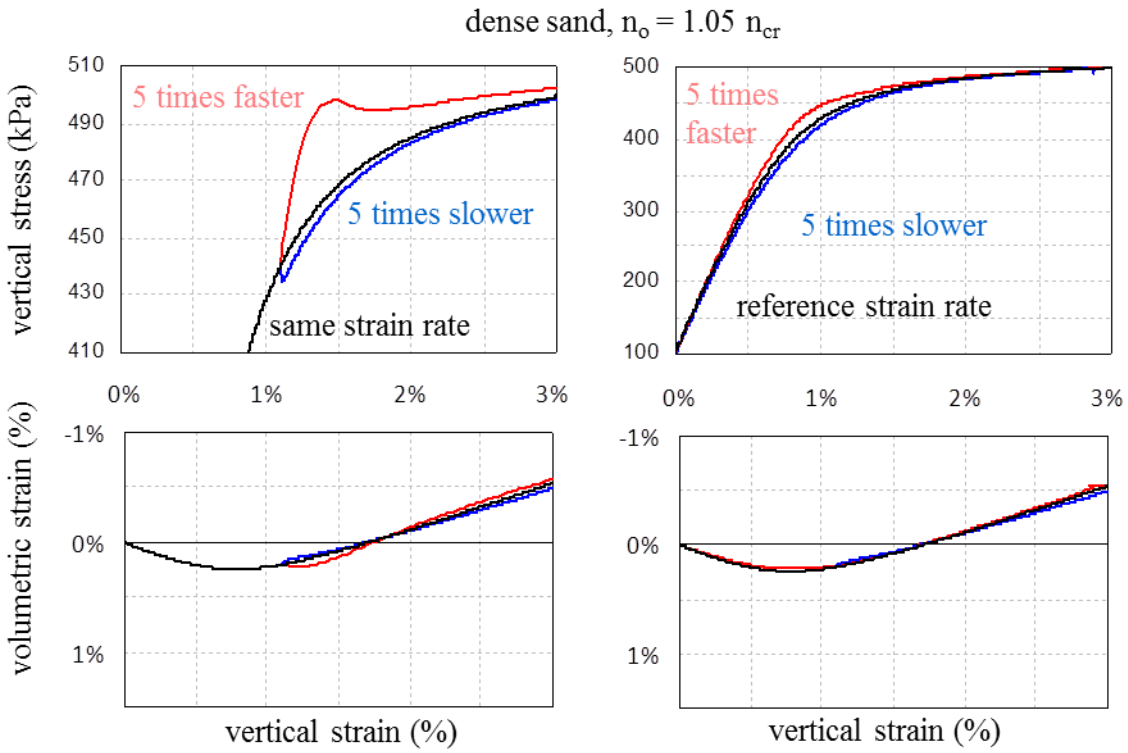

(a) (b)

Figure 7. Strain-controlled triaxial compression tests at constant lateral confining pressure of 100 kPa with constant vertical strain rate of $5x10^{-3}$%/s and (a) stepwise change of the strain rate (5 times slower and 5 times faster) at the same vertical stress and strain levels, and (b) two tests at constant vertical strain rates, one 5 times slower and one 5 times faster.